

Tuning magnetic anisotropy by interfacial engineering in $La_{2/3}Sr_{1/3}Co_{1-x}Mn_xO_{2.5+\delta}/La_{2/3}Sr_{1/3}MnO_3/La_{2/3}Sr_{1/3}Co_{1-x}Mn_xO_{2.5+\delta}$ trilayers

Hai-Lin Huang(黄海林), Liang Zhu(朱亮), Hui Zhang(张慧), Jin-E Zhang(张金娥), Fu-Rong Han(韩福荣), Jing-Hua Song(宋京华), Xiaobing Chen(陈晓冰), Yuan-Sha Chen(陈沅沙), Jian-Wang Cai(蔡建旺), Xue-Dong Bai(白雪冬), Feng-Xia Hu(胡凤霞), Bao-Gen Shen(沈保根), Ji-Rong Sun(孙继荣)

Citation: Chin. Phys. B . 2020, 29(9): 097402 . **doi:** 10.1088/1674-1056/aba2e2

Journal homepage: http://cpb.iphy.ac.cn; http://iopscience.iop.org/cpb

What follows is a list of articles you may be interested in

Thickness-dependent magnetic anisotropy in obliquely deposited Fe(001)/Pd thin film bilayers probed by VNA-FMR

Qeemat Gul, Wei He(何为), Yan Li(李岩), Rui Sun(孙瑞), Na Li(李娜), Xu Yang(杨旭), Yang Li(李阳), Zi-Zhao Gong(弓子召), Zong-Kai Xie(谢宗凯), Xiang-Qun Zhang(张向群), Zhao-Hua Cheng(成昭华)

Chin. Phys. B . 2019, 28(7): 077502 . **doi:** 10.1088/1674-1056/28/7/077502

Thickness dependent manipulation of uniaxial magnetic anisotropy in Fe-thin films by oblique deposition

Qeemat Gul, Wei He(何为), Yan Li(李岩), Rui Sun(孙瑞), Na Li(李娜), Xu Yang(杨旭), Yang Li(李阳), Zi-Zhao Gong(弓子召), ZongKai Xie(谢宗凯), Xiang-Qun Zhang(张向群), Zhao-Hua Cheng(成昭华)

Chin. Phys. B . 2018, 27(9): 097504 . **doi:** 10.1088/1674-1056/27/9/097504

Diverse features of magnetization curves of uniaxial crystals: A simulation study

Hala A. Sobh, Samy H. Aly

Chin. Phys. B . 2017, 26(1): 017503 . **doi:** 10.1088/1674-1056/26/1/017503

Manipulating magnetic anisotropies of Co/MgO(001) ultrathin films via oblique deposition

Syed Sheraz Ahmad, Wei He(何为), Jin Tang(汤进), Yong Sheng Zhang(张永圣), Bo Hu(胡泊), Jun Ye(叶军), Qeemat Gul, Xiang-Qun Zhang(张向群), Zhao-Hua Cheng(成昭华)

Chin. Phys. B . 2016, 25(9): 097501 . **doi:** 10.1088/1674-1056/25/9/097501

Study of magnetization reversal and anisotropy of single crystalline ultrathin Fe/MgO (001) film by magneto-optic Kerr effect

Miao-Ling Zhang(张苗玲), Jun Ye(叶军), Rui Liu(刘锐), Shu Mi(米菽), Yong Xie(谢勇), Hao-Liang Liu(刘郝亮), Chris Van Haesendonck, Zi-Yu Chen(陈子瑜)

Chin. Phys. B . 2016, 25(4): 047503 . **doi:** 10.1088/1674-1056/25/4/047503

Tuning magnetic anisotropy by interfacial engineering in $La_{2/3}Sr_{1/3}Co_{1-x}Mn_xO_{2.5+\delta}/La_{2/3}Sr_{1/3}MnO_3/La_{2/3}Sr_{1/3}Co_{1-x}Mn_xO_{2.5+\delta}$ trilayers*

Hai-Lin Huang(黄海林)[1,2], Liang Zhu(朱亮)[1,2], Hui Zhang(张慧)[1,2], Jin-E Zhang(张金娥)[1,2], Fu-Rong Han(韩福荣)[1,2], Jing-Hua Song(宋京华)[1,2], Xiaobing Chen(陈晓冰)[1,2], Yuan-Sha Chen(陈沅沙)[1,2], Jian-Wang Cai(蔡建旺)[1,2], Xue-Dong Bai(白雪冬)[1,2], Feng-Xia Hu(胡凤霞)[1,2], Bao-Gen Shen(沈保根)[1,2,3], and Ji-Rong Sun(孙继荣)[1,2,3,†]

[1] *Beijing National Laboratory for Condensed Matter Physics & Institute of Physics, Chinese Academy of Sciences, Beijing* 100190, *China*
[2] *School of Physical Sciences, University of Chinese Academy of Sciences, Beijing* 100049, *China*
[3] *Songshan Lake Materials Laboratory, Dongguan* 523808, *China*

(Received 4 June 2020; revised manuscript received 30 June 2020; accepted manuscript online 6 July 2020)

Grouping different oxide materials with coupled charge, spin, and orbital degrees of freedom together to form heterostructures provides a rich playground to explore the emergent interfacial phenomena. The perovskite/brownmillerite heterostructure is particularly interesting since symmetry mismatch may produce considerable interface reconstruction and unexpected physical effects. Here, we systemically study the magnetic anisotropy of tensely strained $La_{2/3}Sr_{1/3}Co_{1-x}Mn_xO_{2.5+\delta}/La_{2/3}Sr_{1/3}MnO_3/La_{2/3}Sr_{1/3}Co_{1-x}Mn_xO_{2.5+\delta}$ trilayers with interface structures changing from perovskite/brownmillerite type to perovskite/perovskite type. Without Mn doping, the initial $La_{2/3}Sr_{1/3}CoO_{2.5+\delta}/La_{2/3}Sr_{1/3}MnO_3/La_{2/3}Sr_{1/3}CoO_{2.5+\delta}$ trilayer with perovskite/brownmillerite interface type exhibits perpendicular magnetic anisotropy and the maximal anisotropy constant is 3.385×10^6 erg/cm^3, which is more than one orders of magnitude larger than that of same strained LSMO film. By increasing the Mn doping concentration, the anisotropy constant displays monotonic reduction and even changes from perpendicular magnetic anisotropy to in-plane magnetic anisotropy, which is possible because of the reduced CoO_4 tetrahedra concentration in the $La_{2/3}Sr_{1/3}Co_{1-x}Mn_xO_{2.5+\delta}$ layers near the interface. Based on the analysis of the x-ray linear dichroism, the orbital reconstruction of Mn ions occurs at the interface of the trilayers and thus results in the controllable magnetic anisotropy.

Keywords: perovskite/brownmillerite heterostructure, magnetic anisotropy, orbital reconstruction

PACS: 74.78.Fk, 75.30.Gw, 75.25.Dk **DOI:** 10.1088/1674-1056/aba2e2

1. Introduction

The interface in complex oxide heterostructure provides a rich playground to explore the emergent interfacial phenomena that arise due to electronic, spin, or orbital reconstruction.[1–7] Tuning interfacial electromagnetic properties by interfacial engineering in oxide heterostructure is crucial for designing the technological applications, such as magnetic tunnel junctions,[8] magnetic-field sensors, and magnetic recording read heads.[9–11] Recently, controllable oxygen octahedron tilt/rotation at interfaces in perovskite oxide heterostructures by interfacial engineering have been intensively studied and fruitful results have been achieved.[12–20] Liao *et al.* reported transferring octahedron rotation from $NdGaO_3$ substrate to ultrathin $La_{2/3}Sr_{1/3}MnO_3$ (LSMO) film.[16] The titling MnO_6 octahedron has modified the hopping rate of the e_g orbital of Mn ions along different axes, causing an in-plane switching of the easy axis of LSMO film by an angle of 90° and giant anisotropic transport properties in the LSMO films. As revealed by Kan *et al.*, Ru–O–Ru bond angle was modified and the magnetic anisotropy (MA) of the entire $SrRuO_3$ layer was tuned by inserting a few-layer $Ca_{0.5}Sr_{0.5}TiO_3$ into the interface of $SrRuO_3/GdScO_3$ heterostructure.[17] As shown by Wang *et al.*, the interfacial Dzyaloshinskii–Moriya interaction was manipulated through ferroelectric proximity effect at the $BaTiO_3/SrRuO_3$ heterointerface, achieving local, switchable, and nonvolatile control of the density and stability of magnetic skyrmions.[20]

In previous works, most of the emergent interfacial phenomena were realized in the perovskite/perovskite (P/P) heterostructures. Due to advances in epitaxial synthesis techniques, grouping oxide materials together with different atomic/electronic configurations is accessible.[21–24] In recent work, Zhang *et al.* demonstrated how symmetry mismatch drives a spin reorientation for the tensile-strained $LSMO/LaCoO_{2.5+\delta}$ multilayers with perovskite/brownmillerite (P/BM) interface.[22] It is found that the interfacial MnO_6 octahedra prefer to share the apical oxygen with neighboring CoO_4 tetrahedra, causing MnO_6 octahedral elongated and tilted, leading to strong perpendic-

*Project supported by the National Basic Research Program of China (Grant Nos. 2016YFA0300701, 2017YFA0206300, 2017YFA0303601, and 2018YFA0305704), the National Natural Science Foundation of China (Grant Nos. 11520101002, 51590880, 11674378, 11934016, and 51972335), and the Key Program of the Chinese Academy of Sciences.

†Corresponding author. E-mail: jrsun@iphy.ac.cn

© 2020 Chinese Physical Society and IOP Publishing Ltd

ular magnetic anisotropy (PMA). We notice that the bulk $La_{2/3}Sr_{1/3}CoO_3$ and LSMO materials are both optimal doping with ferromagnetic metallic character. Different from LSMO, the tensile-strained $La_{2/3}Sr_{1/3}CoO_3$ thin films easily lose oxygen to form ordering of oxygen vacancies, i.e., the brownmillerite structure of $La_{2/3}Sr_{1/3}CoO_{2.5+\delta}$ (LSCO).[25,26] The P/BM interface based heterostructures can be formed by grouping the LSCO and LSMO film together, and such symmetry mismatch at the interface may possibly tune the MA of the LSMO layer. Moreover, using Mn ions to substitute Co ions can effectively modulate the lattice structure of $La_{2/3}Sr_{1/3}Co_{1-x}Mn_xO_{2.5+\delta}$ (LSCMO) film from brownmillerite to perovskite. We are wondering whether the MA would show the corresponding variations when the interface structure gradually changes from P/BM to P/P-type. Here, we successfully fabricate LSCO/LSMO/LSCO trilayer with the P/BM interface structure. The trilayer exhibits huge PMA and the maximal anisotropy constant is up to $\sim 3.385 \times 10^6$ erg/cm^3 at 10 K, which is more than one order of magnitude larger than that of magnetoelastic coupling effect.[16,27–29] Using Mn ions to substitute Co ions to form LSCMO ($x = 0$–0.7) layers with reduced CoO_4 tetrahedra concentration at the interface, we can tune the type of interface structure for LSCMO/LSMO/LSCMO ($x = 0$–0.7) trilayers from P/BM to P/P, which is confirmed by the high-resolution scanning transmission electron microscope (STEM). The MA of the trilayers displays a strong dependence on the concentration of Mn ions. The K_A of trilayers monotonously decreases as Mn concentration increases and changes from 3.385×10^6 erg/cm^3 to -3.501×10^6 erg/cm^3. The x-ray linear dichroism (XLD) results reveal that the orbital reconstruction occurs at the interface of the trilayers, resulting in the changes in MA due to the strong spin–orbit coupling effect. This work demonstrates the great potential to tune the electromagnetic properties of oxide heterostructure by interfacial engineering.

2. Experiment

LSCMO(6 nm)/LSMO(6 nm)/LSCMO(6 nm) ($x = 0$–0.7) trilayers, [LSCO(4 uc)/LSMO(4 uc)]$_5$ and [LSCMO(4 uc) / LSMO(4 uc)]$_5$ ($x = 0.7$) superlattices were grown on (001)-$SrTiO_3$ (STO) single crystal substrates ($3\times5\times0.5$ mm^3) by pulsed laser deposition, using a KrF excimer laser with a wavelength of 248 nm. The fluence of the laser pulse was 2 J/cm^2 and the repetition rate was 2 Hz. The deposition was carried out at 680 ℃ in an oxygen atmosphere of 30 Pa for the LSMO layer and LSCMO layers. The distance between the polycrystalline target and substrate is ~ 4.8 cm. The growth rate is ~ 2 nm/min for the LSMO layer and ~ 1.4 nm/min for LSCMO layers. After deposition, the samples were cooled to room temperature at a rate of 10 ℃/min in an oxygen atmosphere of 100 Pa. The film thickness was determined by the number of laser pulses, which has been carefully calibrated by the technique of small angle x-ray reflectivity.

The surface morphology of the trilayers was measured by an atomic force microscope (SPI 3800 N, Seiko). X-ray diffraction (XRD) and reciprocal space mapping (RSM) was determined by Bruker x-ray diffractometer (D8 discover). High-angle annular dark-field (HAADF) images were recorded by a high-resolution STEM with double Cs correctors (JEOL-ARM200 F). Magnetic measurements were conducted by a quantum designed vibrating sample magnetometer (VSM-SQUID) in the temperature interval from 10 K to 380 K. The x-ray absorption spectra (XAS) were performed at Shanghai Synchrotron Radiation Facility, in the total electron yield mode. The spectra were measured at the Mn L-edge for the two polarizations in a geometry. The x-ray incident angle was rotated to 0° and 60° from the sample normal, which correspond to the in-plane ($E||a$, I_{IP}) and out-of-plane ($E||c$, I_{OP}) directions, respectively. The x-ray linear dichroism spectra, defined by I_{IP}–I_{OP}, was the intensity difference of normalized XAS along two polarizations, which provide information about the orbital occupancy of Mn-3d states. The measurement temperature was 300 K.

3. Results and discussion

High-quality LSCMO/LSMO/LSCMO ($x = 0$–0.7) trilayers are epitaxially grown on single-crystalline STO substrate, and the schematic diagram of the trilayers is shown in Fig. 1(a). Here, the thicknesses of the LSCMO layers and LSMO layer are fixed to 6 nm, which will highlight the interfacial effect of the trilayers.[22] The thickness of trilayers is confirmed by low-angle x-ray reflectivity (Fig. S1). All trilayers display an atomical flat surface. Figure 1(b) shows the typical surface morphology of LSCO/LSMO/LSCO trilayer with the root mean square roughness of ~ 0.3 nm, measured over an area of 5×5 μm^2. The lattice constant is 3.87 Å for pseudo-cubic LSMO[27–29] and 3.83–3.87 Å for pseudo-cubic LSCMO materials,[30] both of which are smaller than that of the STO substrate (3.905 Å). This indicates that the LSCMO/LSMO/LSCMO trilayers will be tensely strained to the STO substrate. It has been confirmed by the (002) Bragg peaks of trilayers that are localized on the right side of the STO substrate as shown in Fig. 1(c). Here, the multi-peaks of trilayers are due to the diffraction/interference of x-ray in the three layers of the heterostructures, which are usually a signature of high crystal quality of the multilayer films. To determine the strain values for each trilayer, we simulate all the XRD patterns of the trilayers, and the fitting curves (blue curve) of XRD patterns are well consistent with the experimental results (Fig. S2(a)). The lattice constant of the LSCMO ($x = 0$–1) layers can be deduced from these fitting curves as shown in Fig. S2(b). The out-of-plane lattice constant of the LSCMO

layers shows a monotonic increase as the Mn doping concentration increases (from 3.75 Å for LSCO to 3.84 Å for LSCMO ($x = 0.7$)), whereas the out-of-plane lattice constant of the LSMO layer maintains a constant value of 3.85 Å. It means that each trilayer sample always suffers from the tensile strain from the STO substrate. To elucidate the tensile strain state of the trilayers, the typical RSMs around asymmetric $(\bar{1}03)$ reflection of LSCO/LSMO/LSCO and LSCMO/LSMO/LSCMO ($x = 0.7$) trilayers are shown in Figs. 1(d) and 1(e), respectively. The reflections from the trilayers not only align vertically with that of the substrate (marked by dashed lines) but also above that of the substrate, indicating the trilayers are coherently strained by the substrate without any lattice relaxation. Similar results are obtained for other trilayers.

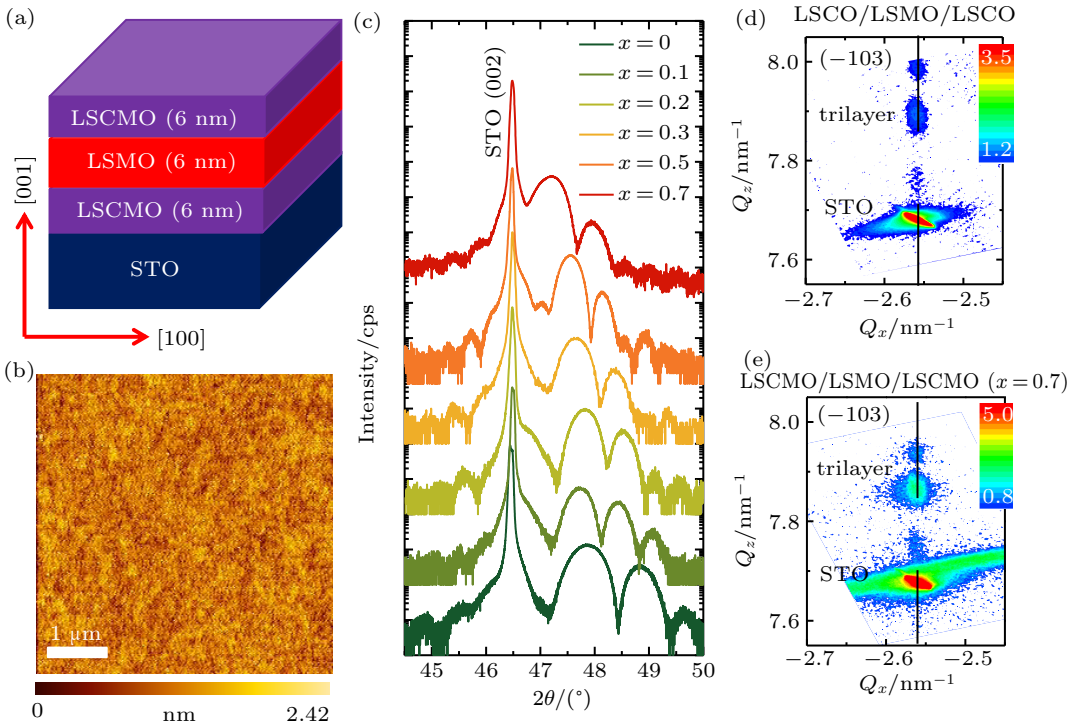


Fig. 1. (a) The sketch diagram of LSCMO/LSMO/LSCMO ($x = 0$–0.7) trilayers. (b) The surface morphology of the LSCO/LSMO/LSCO trilayer; the scale of the image is 5×5 μm^2. (c) The x-ray diffraction patterns of LSCMO/LSMO/LSCMO trilayers. The multi-peaks indicate the high crystal quality of the trilayers. The reciprocal space mappings of the $(\bar{1}03)$ reflections of (d) LSCO/LSMO/LSCO and (e) LSCMO/LSMO/LSCMO ($x = 0.7$) trilayers.

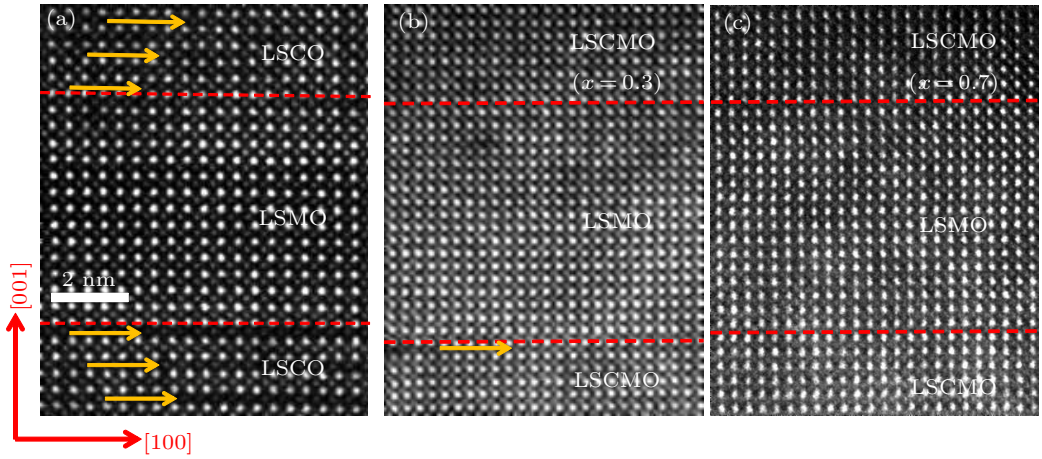


Fig. 2. Typical high-angle annular dark-field image of the cross-section of the LSCMO/LSMO/LSCMO trilayers with (a) $x = 0$, (b) $x = 0.3$, and (c) $x = 0.7$, respectively, recorded along the [100] zone. Red dashed-line marks the LSCMO/LSMO interface and the yellow arrows represent the dark stripes.

To obtain detailed information about the lattice structure of LSCMO/LSMO/LSCMO trilayers, figures 2(a)–2(c) presents the typical HAADF images of the cross-section of the LSCMO/LSMO/LSCMO ($x = 0$, 0.3, 0.7) trilayers, recorded along the [100] zone axis. Here, the brighter spots are La/Sr ions and the fainter spots are Mn/Co ions. At first glance, the interface of LSCMO/LSMO in the trilayers is sharp and the LSMO layer displays the perovskite structure without any defects. However, dark stripes appear every two columns in the LSCO layers, indicating the formation of the brownmil-

lerite LSCO phase.[21–24] Notably, the dark stripe favors the position near the LSMO layer, indicating that the interface of the LSCO/LSMO/LSCO trilayer is the P/BM type as shown in Fig. 2(a). On the contrary, for the LSCMO/LSMO/LSCMO ($x = 0.3$) trilayer, only a few dark stripes at the interface of LSCMO ($x = 0.3$) layers are observed, which means that the P/BM interface is reduced and P/P interface is increased, as shown in Fig. 2(b). For the LSCMO/LSMO/LSCMO ($x = 0.7$) trilayer, no dark stripe is observed, which means that the interface of trilayer is completely P/P structure, as shown in Fig. 2(c). The STEM results indicate that we successfully change the interface structure of LSCMO/LSMO/LSCMO trilayers from P/BM to P/P structure.

It is interesting to see whether the different interface structures will influence the MA of the LSCMO/LSMO/LSCMO trilayers. So we pay our attention to the magnetic properties of the trilayers. Figure 3(a) shows the thermomagnetic (M–T) curves of LSCO/LSMO/LSCO trilayer with P/BM interface along in-plane (IP) and out-of-plane (OP) applied fields at various magnetic fields with field-cooling mode, respectively. Taking the data with the field of 0.05 T as an example, the magnetic moment first undergoes an obvious increase at the Curie temperature (T_c) of the LSMO layer (the increase-to-decrease crossover at $\sim$ 235 K is an indication of the spin reorientation), and then rapidly drops along the IP direction upon cooling. Meanwhile, the magnetic moment of OP direction exhibits monotonous increase upon cooling, and the magnetic moment of OP direction is about 4 times larger than that of the IP one at 10 K. As the magnetic field increases, the IP M–T curves gradually approach that of OP direction, and the spin reorientation phenomena can still be clearly seen in the M–T curve under the applied field of 1.5 T. The M–T curves clearly manifest an easy axis of the LSCO/LSMO/LSCO trilayer along OP direction. Compared to the PMA of the LSCO/LSMO/LSCO trilayer, the LSCMO/LSMO/LSCMO ($x = 0.7$) trilayer with the P/P interface displays a totally different MA. Figure 3(b) presents the M–T curves of LSCMO/LSMO/LSCMO ($x = 0.7$) trilayer along IP and OP applied fields at various magnetic fields. The magnetic moments of two directions monotonously increase upon cooling and no spin reorientation phenomena are observed. The magnetic moment of OP direction gradually approaches that of IP direction as the applied fields increase, and they become almost coincide at 1.5 T. These results manifest the easy axis of the LSCMO/LSMO/LSCMO ($x = 0.7$) trilayer along the IP direction.

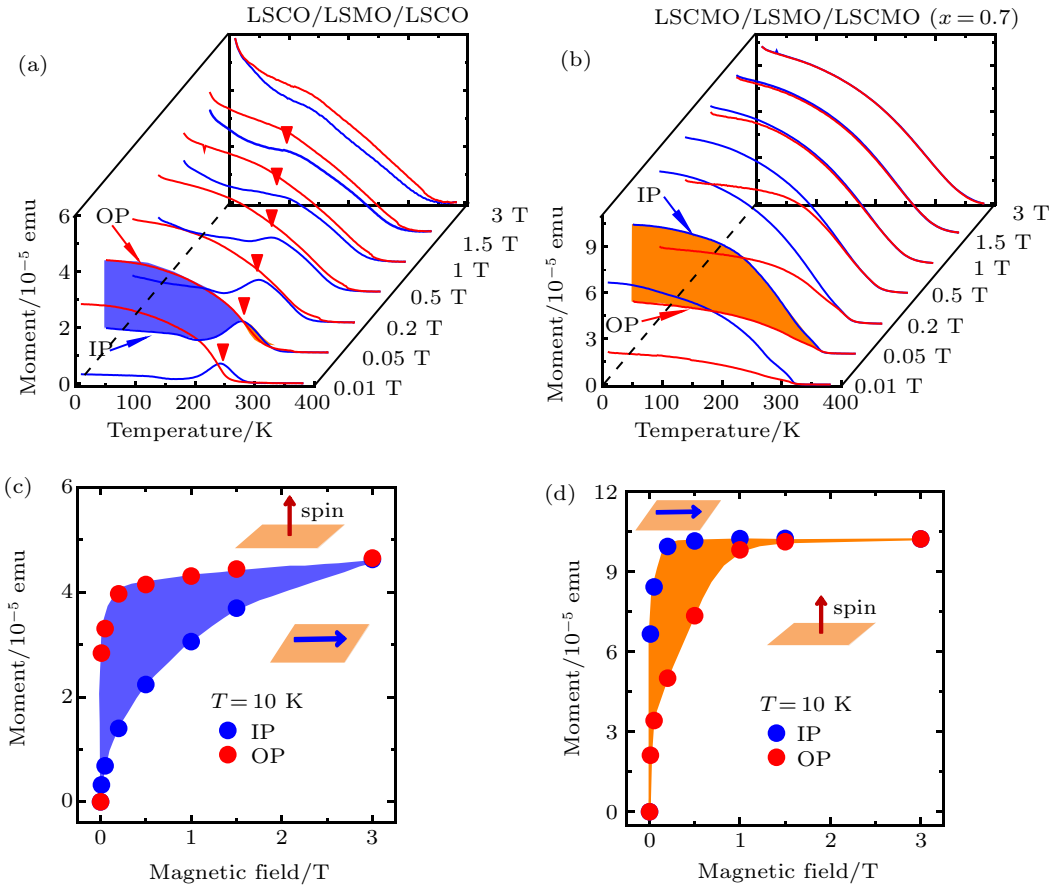


Fig. 3. Thermomagnetic curves of the (a) LSCO/LSMO/LSCO and (b) LSCMO/LSMO/LSCMO ($x = 0.7$) trilayers. The data were acquired in field-cooling mode with in-plane or out-of-plane applied fields. Blue and orange areas highlight the difference of the magnetic moments along two measuring directions. The moment as a function of applied fields for the (c) LSCO/LSMO/LSCO and (d) LSCMO/LSMO/LSCMO ($x = 0.7$) trilayers, extracted from the thermomagnetic data at $T = 10$ K. The shaded area corresponds to the energy required to orientate the magnetic moment of trilayer from the hard axis to the easy axis.

To obtain the quantitative description of MA, the anisotropy constant (K_A) is calculated. Figure 3(c) presents the magnetic moment as a function of the magnetic field (M–H curves), extracted from the M–T curves of LSCO/LSMO/LSCO trilayer along IP and OP directions at 10 K. Along the OP direction, the magnetic moment increases rapidly with the applied field and saturates in a field about 0.2 T. In contrast, the magnetic moment exhibits a smooth growth with applied field along the IP direction. The energy required to force IP magnetic moment to align with the OP direction equals the shaded area encircled by the M–H curves. The calculation gives $\sim 3.385 \times 10^6$ erg/cm^3 of the K_A for LSCO/LSMO/LSCO trilayer at 10 K, which is more than one order of magnitude larger than that of bare LSMO film with magnetoelastic coupling interaction ($\sim 10^4$ erg/cm^3).[16,25–27] Here, the positive value of K_A stands for the PMA of trilayers. Following the same procedure, the M–H curve of LSCMO/LSMO/LSCMO ($x = 0.7$) trilayer at 10 K is obtained as shown in Fig. 3(d). The IP magnetic moment increases rapidly with the applied field and saturates in a field about 0.2 T along the IP direction, while the OP magnetic moment quickly increases with the applied field and almost saturates in a field about 1.5 T. The K_A of LSCMO/LSMO/LSCMO ($x = 0.7$) trilayer at 10 K is $\sim -3.501 \times 10^6$ erg/cm^3. Following the same calculation procedure, the K_A values of the LSCO/LSMO/LSCO and LSCMO/LSMO/LSCMO ($x = 0.7$) trilayers at other temperatures are obtained and the results will discuss later.

To explore the MA variation of the tensile-strained LSCMO/LSMO/LSCMO ($x = 0$–0.7) trilayers on the gradually changed interface structure from P/BM to P/P-type, a series of M–T curves of other LSCMO/LSMO/LSCMO ($x = 0$–0.7) trilayers are measured at different applied fields (Fig. S3). To show the changing tendency of the magnetic behavior of the trilayers, figure 4(a) presents the typical M–T curves of the LSCMO/LSMO/LSCMO ($x = 0$–0.7) trilayers under the applied field of 0.05 T. When $x \leq 0.3$, the magnetic moment of IP direction is below that of OP direction at low temperature, and the magnetic moments of two directions gradually approach as x increases from 0 to 0.3, indicating the tendency of PMA to decrease as x increases. When $x \geq 0.5$, the easy axis of the trilayers is turned to the IP direction, i.e., the magnetic moment of the IP direction is bigger than that of the OP one. The K_A values as a function of temperature for the LSCMO/LSMO/LSCMO ($x = 0$–0.7) trilayers are summarized, as shown in Fig. 4(b); the absolute value of K_A decreases gradually as the temperature increases. To clearly display the LSCMO layers effect MA of the trilayers, figure 4(c) shows the K_A of the LSCMO/LSMO/LSCMO ($x = 0$–0.7) trilayers at 10 K. The K_A of trilayers displays a strong dependence on Mn concentration, and it monotonously decreases and changes from 3.385×10^6 erg/cm^3 to -3.501×10^6 erg/cm^3. The K_A of trilayers is positive as $x \leq 0.3$ and it becomes negative as $x \geq 0.5$, indicating that the easy axis of the trilayers prefers OP direction as $x \leq 0.3$ and it reverses to the IP direction as $x \geq 0.5$. The easy axes of the LSCMO/LSMO/LSCMO ($x = 0$–0.7) trilayers are further confirmed by directly measuring hysteresis loops with IP and OP applied fields (Fig. S4), and the value of K_A from hysteresis loops of the trilayers is also calculated (Fig. 4(c)). Two calculation methods agree well with each other, indicating that the value of K_A is reliable. As demonstrated above, the easy axis of the trilayers changes from OP direction to IP direction as the interface structure ranges from P/BM to P/P-type.

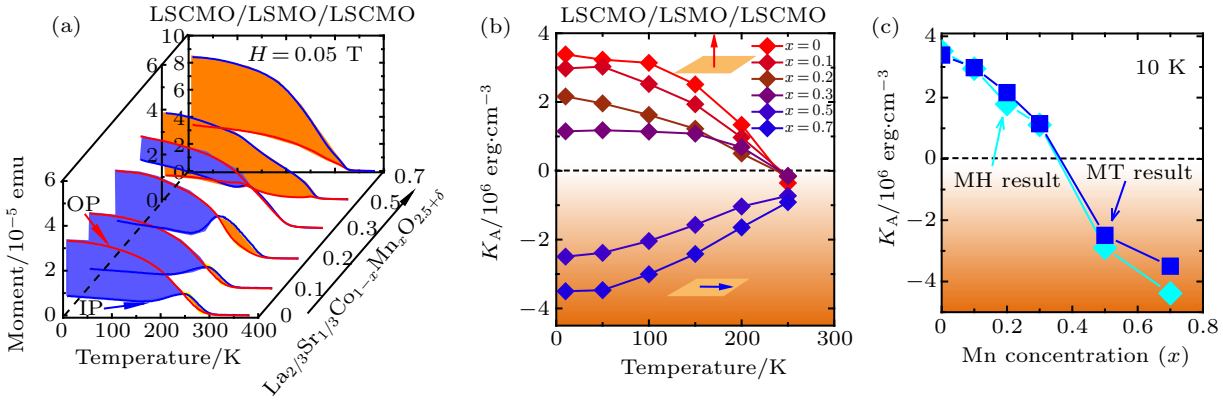


Fig. 4. (a) Thermomagnetic curves of the LSCMO/LSMO/LSCMO ($x = 0$–0.7) trilayers along the in-plane and out-of plane directions under an applied field of 0.05 T. (b) The K_A as a function of temperature for the LSCMO/LSMO/LSCMO ($x = 0$–0.7) trilayers. Here, the positive value of K_A indicates the perpendicular magnetic anisotropy. (c) The K_A as a function of Mn concentration for the LSCMO/LSMO/LSCMO ($x = 0$–0.7) trilayers at 10 K. The blue curve and light green curve are the results extracted from thermomagnetic curves and hysteresis curves, respectively.

It is already known that the electron filling of 3d-orbitals of transition metal oxides plays a crucial role to determine the electric and magnetic properties of oxide heterostructures.[31–35] In order to obtain the information on electron occupancy of Mn-3d orbital of the trilayers, the technique of XAS is adopted. Fig-

ures 5(a) and 5(b) present the the normalized XAS spectra for the samples of [LSCO(4 uc)/LSMO(4 uc)]$_5$ and [LSCMO(4 uc)/LSMO(4 uc)]$_5$ ($x = 0.7$) multilayers, respectively. Here, the multilayers with an ultrathin layer thickness (4 uc) were chosen to highlight the interface effect. The sketch of XAS measurement with two optical polarizations (0° and 60° from the sample normal) is shown at the upper right position in Fig. 5(a), corresponding to the in-plane ($E||a$, I_{IP}) and out-of-plane ($E||c$, I_{OP}) directions. The Mn-$L_{2,3}$ edges spectra consist of two main peaks, which are due to the excited electron from the spin–orbit split $2p_{1/2}$ and $2p_{3/2}$ core levels to empty 3d orbital states, and the Mn-L_2 peak contains important information about electron occupancy of e_g-orbitals: a high (low) peak implies a low (high) orbital occupancy.[36–40] To intuitively present the electron occupancy of e_g-orbitals in the multilayers, XLD spectra, defined by I_{IP}–I_{OP}, are obtained. The positive (negative) value means that electron preferentially occupies $d_{3z^2-r^2}$ ($d_{x^2-y^2}$) orbital of the Mn ions. For [LSCO/LSMO]$_5$ multilayer, the XLD spectrum exhibits positive value around the Mn-L_2 spectrum, indicating that more electron preferentially occupy $d_{3z^2-r^2}$ orbital. This is understandable because the BM/P interface of the [LSCO/LSMO]$_5$ will elongate MnO_6 octahedron along [001] axis, thus lowering the energy level of $d_{3z^2-r^2}$, which is consistent with the previous report.[22,27] In contrast, the orbital occupancy is different in [LSCMO/LSMO]$_5$ ($x = 0.7$) multilayer with P/P-type interface, and the preferred orbital is $d_{x^2-y^2}$ as implied by the negative value of XLD spectra around Mn-L_2 spectra. This result is interesting since it reveals interface orbital reconstruction by interfacial engineering in LSCMO/LSMO/LSCMO trilayers.

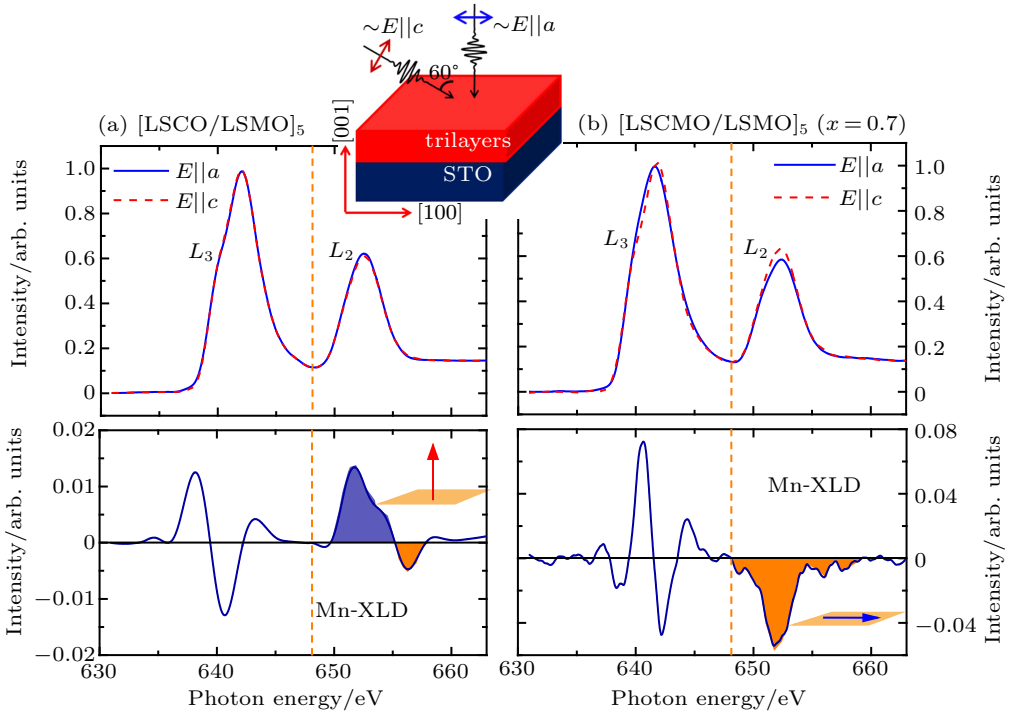


Fig. 5. Normalized Mn-XAS spectra for the (a) [LSCO(4 uc)/LSMO(4 uc)]$_5$ and (b) [LSCMO(4 uc)/LSMO(4 uc)]$_5$ ($x = 0.7$) multilayers, measured with the optical polarization parallel ($E||a$, I_{IP}) or perpendicular ($E||c$, I_{OP}) to the film plane. The sketch shows the experimental setup. Bottom panels are the corresponding XLD spectra and the shaded areas provide the information on orbital occupancy. The arrow marks the spin orientation of the LSMO layer.

The above results strongly suggest that the MA and the orbital reconstruction are closely related to the interfacial coupling effect in the LSCMO/LSMO/LSCMO trilayers. As already demonstrated, the interface type changes from P/BM to P/P as the content of Mn increases. For the P/BM type interface, the interfacial MnO_6 octahedra share the apical oxygen with neighboring CoO_4 tetrahedra at the interface (Fig. 2(a)). This would cause the interfacial MnO_6 octahedra to elongate along the [001] axis and tilt around the [110] axis to accommodate the symmetry mismatch between the CoO_4 layer and the MnO_6 layers.[22] In this case, the $d_{3z^2-r^2}$ orbital will be preferentially occupied, thus leading to the PMA of the trilayers according to the Bruno model (this will be discussed later). In contrast, for the P/P-type interface with oxygen octahedra on both sides, the interface-induced tilt of oxygen octahedra is expected to be small,[16,18] and the magnetoelastic coupling is the major factor to determine orbital occupation. Generally, the tensile strain would cause a preferential occupation of $d_{x^2-y^2}$ orbital in LSMO films, thus causing in-plane magnetic anisotropy.[33,34,38] By increasing the Mn doping concentration in the LSCMO layer, the CoO_4–MnO_6 pairs at the interface are reduced, which results in the monotonic decrease of

K_A of the trilayers and finally, an in-plane anisotropy appears.

A further issue to be addressed is how the orbital reconstruction modifies the MA of the manganite oxide heterojunctions. The LSMO film owns strongly coupled spin, charge, and orbital degrees of freedom, and the MA stems from the strong spin–orbital interaction. According to the Bruno model, the anisotropy of the spin–orbit energy is directly related to the anisotropy of the orbital moment[31,41]

$$\Delta E_{SO} = \zeta\left[\langle \hat{L}\cdot\hat{S}\rangle_{IP} - \langle \hat{L}\cdot\hat{S}\rangle_{OP}\right] = \frac{\zeta}{4\mu_B}\left(m_O^{OP} - m_O^{IP}\right), \quad (1)$$

where ζ is a parameter for spin-orbit coupling, $\langle\ \rangle$ represents the thermodynamic average, and m_O is the d-orbital moment along OP or IP directions (Note 1 for detailed calculations of m_O). For the LSCO/LSMO/LSCO trilayer, the electron preferentially fills $d_{3z^2-r^2}$ orbital of the Mn ions, and a direct calculation gives that the d-orbital moment is $4\mu_B\zeta/\Delta_{x^2-y^2,xy}$ along the OP direction and $(\mu_B\zeta/\Delta_{x^2-y^2,xz})$ along the IP direction. According to Eq. (1), the easy axis has a larger orbital moment than that of the hard axis. It is obvious that $m_O^{OP} > m_O^{IP}$, which means that the easy axis of LSCO/LSMO/LSCO trilayer is OP direction. For the LSCMO/LSMO/LSCMO ($x = 0.7$) trilayer, the electron preferentially occupies $d_{x^2-y^2}$ orbital, and the corresponding m_O values of d-orbital are 0 and $(3\mu_B\zeta/\Delta_{3z^2-r^2,xz})$ for OP and IP directions, respectively. The $m_O^{OP} < m_O^{IP}$, so the easy axis is reversed along the IP direction for the LSCMO/LSMO/LSCMO ($x = 0.7$) trilayer. Due to the strong spin–orbit coupling effect, the orbital reconstruction occurs at the interface of LSCMO/LSMO/LSCMO trilayers by interfacial engineering, resulting in tuning MA of the trilayers.

4. Conclusion

In summary, we systemically research the MA of tensile-strained LSCMO/LSMO/LSCMO ($x = 0$–0.7) trilayers with the interface structure changing from P/BM to P/P-type. The initial LSCO/LSMO/LSCO with typical P/BM structure exhibits huge PMA and the maximal value of K_A is $\sim 3.385\times 10^6$ erg/cm^3 at 10 K, which is more than one order of magnitude larger than that of tensile-strained LSMO film. Using Mn ions to substitute Co ions of LSCO layer to reduce the CoO_4 tetrahedra concentration of the LSCMO layers, the value of K_A of trilayers changes from 3.385×10^6 erg/cm^3 to -3.501×10^6 erg/cm^3. When $x \le 0.3$, PMA dominates and the value of K_A monotonously decreases as Mn concentration increases. However, in-plane MA dominates as $x \ge 0.5$, i.e., the easy magnetic axis of trilayers changes from OP to IP directions. The orbital reconstruction occurs at the interface of the LSCMO/LSMO/LSCMO trilayers by interfacial engineering, resulting in the change of MA due to the strong spin–orbit coupling effect. Thus, this work demonstrates the great potential to tune the electromagnetism properties of oxide heterostructure by interfacial engineering.

References

[1] Okamoto S and Millis A J 2004 *Nature* **428** 630
[2] Chakhalian J, Freeland J W, Habermeier H U, Cristiani G, Khaliullin G, van Veenendaal M and Keimer B 2007 *Science* **318** 1114
[3] Zubko P, Gariglio S, Gabay M, Ghosez P and Triscone J M 2011 *Annu. Rev. Condens. Matter Phys.* **2** 141
[4] Hwang H Y, Iwasa Y, Kawasaki M, Keimer B, Nagaosa N and Tokura Y 2012 *Nat. Mater.* **11** 103
[5] Cui B, Song C, Li F, Wang G Y, Mao H J, Peng J J, Zeng F and Pan F 2015 *Sci. Rep.* **4** 4206
[6] Bhattacharya A and May S J 2014 *Annu. Rev. Mater. Res.* **44** 65
[7] Hellman F, Hoffmann A, Tserkovnyak Y *et al.* 2017 *Rev. Mod. Phys.* **89** 025006
[8] Dieny B and Chshiev M 2017 *Rev. Mod. Phys.* **89** 025008
[9] Chappert C, Fert A and Van Dau F N 2007 *Nat. Mater.* **6** 813
[10] Ngai J H, Walker F J and Ahn C H 2014 *Annu. Rev. Mater. Res.* **44** 1
[11] Kent A D and Worledge D C 2015 *Nat. Nanotechnol.* **10** 187
[12] He J, Borisevich A, Kalinin S V, Pennycook S J and Pantelides S T 2010 *Phys. Rev. Lett.* **105** 227203
[13] Rondinelli J M, May S J and Freeland J W 2012 *MRS Bull.* **37** 261
[14] Aso R, Kan D, Shimakawa Y and Kurata H 2013 *Sci. Rep.* **3** 2214
[15] Aso R, Kan D, Shimakawa Y and Kurata H 2014 *Adv. Funct. Mater.* **24** 5177
[16] Liao Z, Huijben M, Zhong Z, Gauquelin N, Macke S, Green R J, Van Aert S, Verbeeck J, Van Tendeloo G, Held K, Sawatzky G A, Koster G and Rijnders G 2016 *Nat. Mater.* **15** 425
[17] Kan D, Aso R, Sato R, Haruta M, Kurata H and Shimakawa Y 2016 *Nat. Mater.* **15** 432
[18] Yi D, Flint C L, Balakrishnan P P, Mahalingam K, Urwin B, Vailionis A, N'Diaye A T, Shafer P, Arenholz E, Choi Y, Stone K H, Chu J H, Howe B M, Liu J, Fisher I R and Suzuki Y 2017 *Phys. Rev. Lett.* **119** 077201
[19] Ismail-Beigi S, Walker F J, Disa A S, Rabe K M and Ahn C H 2017 *Nat. Rev. Mater.* **2** 17060
[20] Wang L F, Feng Q Y, Kim Y, Kim R, Lee K H, Pollard S D, Shin Y J, Zhou H B, Peng W, Lee D, Meng W J, Yang H, Han J H, Kim M, Lu Q Y and Noh T W 2018 *Nat. Mater.* **17** 1087
[21] Ding J F, Cossu F, Lebedev O I, Zhang Y Q, Zhang Z D, Schwingenschlogl U and Wu T 2016 *Adv. Mater. Interfaces* **3** 1500676
[22] Zhang J, Zhong Z, Guan X, Shen X, Zhang J, Han F, Zhang H, Zhang H, Yan X, Zhang Q, Gu L, Hu F, Yu R, Shen B and Sun J 2018 *Nat. Commun.* **9** 04304
[23] Zhang J E, Han F R, Wang W, Shen X, Zhang J, Zhang H, Huang H L, Zhang H R, Chen X B, Qi S J, Chen Y S, Hu F X, Yan S S, Shen B G, Yu R C and Sun J R 2019 *Phys. Rev. B* **100** 094432
[24] Behera B C, Jana S, Bhat S G, Gauquelin N, Tripathy G, Anil Kumar P S and Samal D 2019 *Phys. Rev. B* **99** 024425
[25] Liu B, Wang Y Q, Liu G J, Feng H L, Yang H W, Xue X Y and Sun J R 2016 *Phys. Rev. B* **93** 094421
[26] Li J, Wang J, Kuang H, Zhang H R, Zhao Y Y, Qiao K M, Wang F, Liu W, Wang W, Peng L C, Zhang Y, Yu R C, Hu F X, Sun J R and Shen B G 2017 *Nanoscale* **9** 13214
[27] Zhang J E, Chen X X, Zhang Q H, Han F R, Zhang J, Zhang H, Zhang H R, Huang H L, Qi S J, Yan X, Gu L, Chen Y S, Hu F X, Yan S S, Liu B G, Shen B G and Sun J R 2018 *ACS Appl. Mater. Interfaces* **10** 40951
[28] Steenbeck K and Hiergeist R 1999 *Appl. Phys. Lett.* **75** 1778
[29] Steenbeck K, Habisreuther T, Dubourdieu C and Sénateur J P 2002 *Appl. Phys. Lett.* **80** 3361
[30] Yang H W, Zhang H R, Li Y, Wang S F, Shen X, Lan Q Q, Meng S, Yu R C, Shen B G and Sun J R 2015 *Sci. Rep.* **4** 06206
[31] Bruno P 1989 *Phys. Rev. B* **39** 865
[32] Huang H B, Shishidou T and Jo T 2000 *J. Phys. Soc. Jpn.* **69** 2399
[33] Huijben M, Martin L W, Chu Y H, Holcomb M B, Yu P, Rijnders G, Blank D H A and Ramesh R 2008 *Phys. Rev. B* **78** 094413

[34] Tebano A, Aruta C, Sanna S, Medaglia P G, Balestrino G, Sidorenko A A, De Renzi R, Ghiringhelli G, Braicovich L, Bisogni V and Brookes N B 2008 *Phys. Rev. Lett.* **100** 137401

[35] Yi D, Lu N P, Chen X G, Shen S C and Yu P 2017 *J. Phys.: Condens. Matter* **29** 443004

[36] Huang D J, Wu W B, Guo G Y, Lin H J, Hou T Y, Chang C F, Chen C T, Fujimori A, Kimura T, Huang H B, Tanaka A and Jo T 2004 *Phys. Rev. Lett.* **92** 087202

[37] Aruta C, Ghiringhelli G, Tebano A, Boggio N G, Brookes N B, Medaglia P G and Balestrino G 2006 *Phys. Rev. B* **73** 235121

[38] Pesquera D, Herranz G, Barla A, Pellegrin E, Bondino F, Magnano E, Sanchez F and Fontcuberta J 2012 *Nat. Commun.* **3** 1189

[39] Peng J, Song C, Li F, Cui B, Mao H, Wang Y, Wang G and Pan F 2015 *ACS Appl. Mat. Interfaces* **7** 17700

[40] Cui B, Li F, Song C, Peng J J, Saleem M S, Gu Y D, Li S N, Wang K L and Pan F 2016 *Phys. Rev. B* **94** 134403

[41] Bruno P, Magnetismus Von Festkörpern und Grenzflächen 1993 *KFA: Jülich Germany*, Chapter **24** 1-p